Solid State Phenomena
ISSN: 1662-9779, Vol. 388, pp 163-170
doi:10.4028/p-PKV0mr

Submitted: 2026-01-19
Revised: 2026-02-16
Accepted: 2026-02-20
Online: 2026-04-15

Global and Local Formability of 3rd Generation Advanced High Strength Steels

Payà Anna[1,a*], Carpio Marcel[1,b], Frómeta David[1,c]

[1]Eurecat, Centre Tecnològic de Catalunya, Unit of Metallic and Ceramic Materials, Plaça de la Ciència, 2, Manresa 08243, Spain

[a*]anna.paya@eurecat.org, [b]marcel.carpio@eurecat.org, [c]david.frometa@eurecat.org

Keywords: sheet metal forming, advanced high strength steels, formability, edge stretching, lightweight design.

Abstract. The present work investigates the global and local formability of two third-generation Advanced High Strength Steels (AHSSs), a quenching & partitioning (Q&P) steel and a Medium Mn (MMn) steel with 1GPa strength. Third-generation Q&P and MMn steels are designed to overcome the limitations of first-generation AHSS grades by enhancing formability while maintaining high mechanical strength, thus enabling more efficient structural design and improved crash performance. Understanding their forming behaviour is essential to ensure their reliable use in complex sheet metal forming operations. In this study, the forming performance of a Q&P and a MMn steel is analysed through experimental procedures involving both in-plane deformation under various loading paths and hole expansion tests with different hole edge qualities, to evaluate their global and local formability. A first-generation Dual Phase (DP) steel is included in the analysis for comparison. The results demonstrate that 3rd Generation Q&P and MMn steels exhibit very good global formability, superior to conventional 1st Generation AHSSs. However, local formability, as evaluated by hole expansion capacity, can be severely compromised by edge manufacturing process. These findings contribute to a deeper understanding of the distinction between global and local formability in third-generation AHSS, offering insights to improve process robustness and support the industrial implementation of these steels in high-performance automotive components.

Introduction

Automotive lightweighting demands materials that reduce mass without compromising crash safety. In this context, third-generation Advanced High Strength Steels (AHSS), especially quenching & partitioning (Q&P) and Medium-Mn (MMn) grades, have been developed to combine tensile strength of around 1 GPa with improved formability, enabling thinner sheets in body-in-white applications [1–4]. Without entering detailed metallurgy, both families share a fine multiphase structure combining ferrite, bainite or tempered martensite with retained austenite (RA). During forming, metastable RA can transform to martensite (Transformation-Induced Plasticity or TRIP effect), enhancing strain hardening capacity and supporting a favourable strength ductility balance in sheet operations [1–3].

For sheet forming design, it is useful to separate global formability from local formability. Global formability describes the ability to avoid localised necking under homogeneously distributed strains in large areas and is typically characterised by the Forming Limit Curve (FLC) and conventional uniaxial tensile metrics. Local formability, in contrast, concerns resistance to fracture under highly concentrated deformation, as found in stretch-flanging, hole extrusion, or tight-radius bending. In these modes, necking-based criteria generally fail, and fracture can occur below the FLC, motivating the use of local/global formability maps and performance indices that combine uniform strain with true fracture/thickness strain to better discriminate AHSS behaviour across stress states and strain paths [5–7].

A widely used measure of local edge performance is the Hole Expansion Ratio (HER). HER is highly sensitive to edge conditions and tooling parameters. The hole fabrication route (mechanical piercing versus laser/EDM), die clearance, and punch geometry alter the damaged zone at the cut edge and thus govern crack initiation and propagation during expansion. Consequently, optimised

edge preparation/tooling can increase HER and delay edge cracking, while microstructural features (phase distribution, hardness gradients, banding) set the intrinsic resistance to microcrack formation at the edge [8–10].

In this study, we compare global and local formability of a Q&P steel and a MMn steel (1 GPa) with a first-generation Dual Phase (DP) steel used for reference. The global formability response is assessed using in-plane deformation under different loading paths using Nakajima stretching tests, and the local response is measured by hole expansion tests with different edge qualities representative of production. The results are interpreted within local/global formability concepts to (i) demonstrate the global formability advantage of third-generation AHSS at similar strength and (ii) quantify the strong sensitivity of edge formability to edge manufacturing, informing process-robust choices of material and cutting/tooling for high-performance automotive components [5–9].

Materials

The materials analysed in this study are three cold-rolled steel sheets at a 1 GPa strength level: two 3rd Gen AHSS, a Medium-Mn (MMn1000) and a Quenching & Partitioning (QP980), both at 1.50 mm nominal thickness, and a Dual Phase (DP1000) reference at 1.40 mm.

The QP980 sheet is representative of Q&P processed multiphase structures with retained austenite stabilised by carbon partitioning, designed to achieve high strength with improved formability [1]. The microstructural components include ferrite, bainitic/ferrite, tempered martensite and RA (14.7% vol. fraction). The MMn1000 sheet presents an ultrafine dual-phase microstructure consisting of ferrite and RA (41% vol. fraction). RA fraction and stability are tuned by intercritical annealing, enabling transformation-assisted deformation and a favourable strength ductility balance [2]. The DP1000 reference exhibits the typical ferrite matrix with martensite islands and RA (2% vol. fraction) of conventional AHSS used in automotive forming and serves here as a benchmark at similar strength [3].

Mechanical properties for each material grade were determined according to UNE EN ISO 6892-1[11] in the transverse direction with respect to the rolling direction because this orientation is more sensitive to anisotropy introduced during rolling and therefore provides a conservative evaluation of the mechanical behaviour. The obtained results are reported in Table 1, which summarizes the mechanical properties of the investigated steel grades. The table includes the material thickness **t**, the yield strength $\boldsymbol{\sigma_{YS}}$, the ultimate tensile strength $\boldsymbol{\sigma_{UTS}}$, the uniform elongation A_g (defined as the elongation at σ_{UTS}), the elongation at fracture A_{80} measured on an initial gauge length of 80mm, and the strain hardening exponent n. The n-value was calculated at different deformation ranges depending on the steel grade (2-4% deformation for DP1000, 2-25% for MMn1000 and 2-14% for QP980).

Table 1. Mechanical properties of the investigated steel grades at transverse direction.

Steel denomination	t [mm]	σ_{YS} [MPa]	σ_{UTS} [MPa]	A_g [%]	A_{80} [%]	n
DP1000	1.4	769	1040	5.3	8.7	0.09
MMn1000	1.5	643	960	25.7	29.6	0.25
QP980	1.5	658	992	14.4	19.0	0.19

Experimental Procedure

Forming Limit Curve (FLC) Determination

Nakajima tests were performed according to ISO 12004-2[12]. The specimens were machined by electrical discharge machining (EDM) considering the less favourable direction of the material, with the shaft oriented 90º with respect to the rolling direction, as indicated in ISO 12004. For the evaluation of the FLC, three valid samples of each geometry were used. Five strain paths were investigated: plane strain ($\varepsilon_2/\varepsilon_1$=0), biaxial strain ($\varepsilon_2/\varepsilon_1$=1) and three deformation paths between uniaxial strain ($\varepsilon_2/\varepsilon_1$=-0.5) and plane strain, where ε_1 and ε_2 are the major and minor strain,

respectively. The geometries of the specimens used to determine the FLC are shown in Fig. 1a. A Nakajima tool with a punch diameter of 100 mm was used to perform the tests. The tests were carried out in a double-acting hydraulic press using a punch speed of 1.0 mm/s. The press holder was equipped with a circular rib to avoid sliding. The deformation was monitored by using a 3D DIC (Digital Image Correlation) equipment integrated into the press (Fig. 1b) [13].

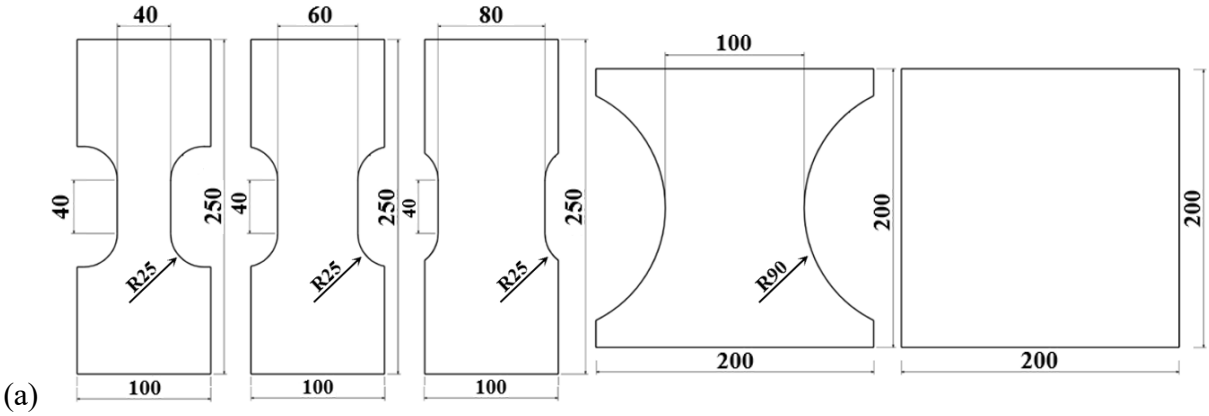

(a)

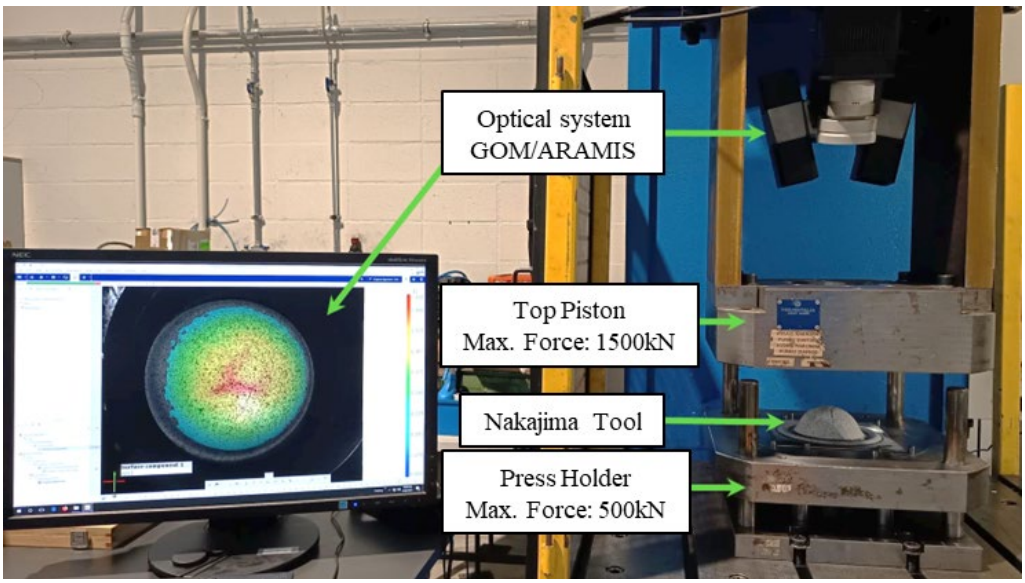

(b)

Fig. 1. (a) Dimensions of the specimens used to determine FLC with a 100mm Nakajima tool; (b) experimental setup for FLC evaluation using a DIC System integrated into the press.

Hole Expansion Tests (HET)

Hole Expansion Tests were performed according to ISO 16630 [14]. Squared samples of 100 × 100 mm were prepared with an initial hole diameter of 10 mm (Fig. 2a) under two different conditions: holes produced by punching using a punch-to-die clearance of 12 ± 1%, following standard recommendations, and holes machined by Electrical Discharge Machining (EDM) to ensure minimal edge damage and burr-free surfaces. The use of EDM holes was intended to provide a reference condition with negligible edge defects, allowing the evaluation of the influence of edge quality on the hole expansion performance [15]. For the expansion tests, a conical expansion tool with a top angle of 60º was used. A schematic representation for the determination of the Hole Expansion Ratio (HER) is shown in Fig. 2b-c. The tests were performed with a constant punch displacement rate of 1 mm/s. A clamping force of 50kN was applied to prevent any material draw-in from the clamping area during the test. All the tests were carried out at room temperature (RT ≈ 25°C). To detect the first sign of cracking, a video camera was positioned at the bottom of the test tool (Fig. 2e). The final diameter was measured using the images obtained when the first crack extended through the thickness of the test piece (Fig. 2d). Using this diameter, the limiting hole expansion was calculated according to the following equation:

$$\lambda = \frac{D_h - D_0}{D_0} x100 \quad (1)$$

Where λ is the limiting hole expansion ratio as a percentage, D_0 is the original hole diameter (10mm), and D_h is the hole diameter after rupture, in millimetres.

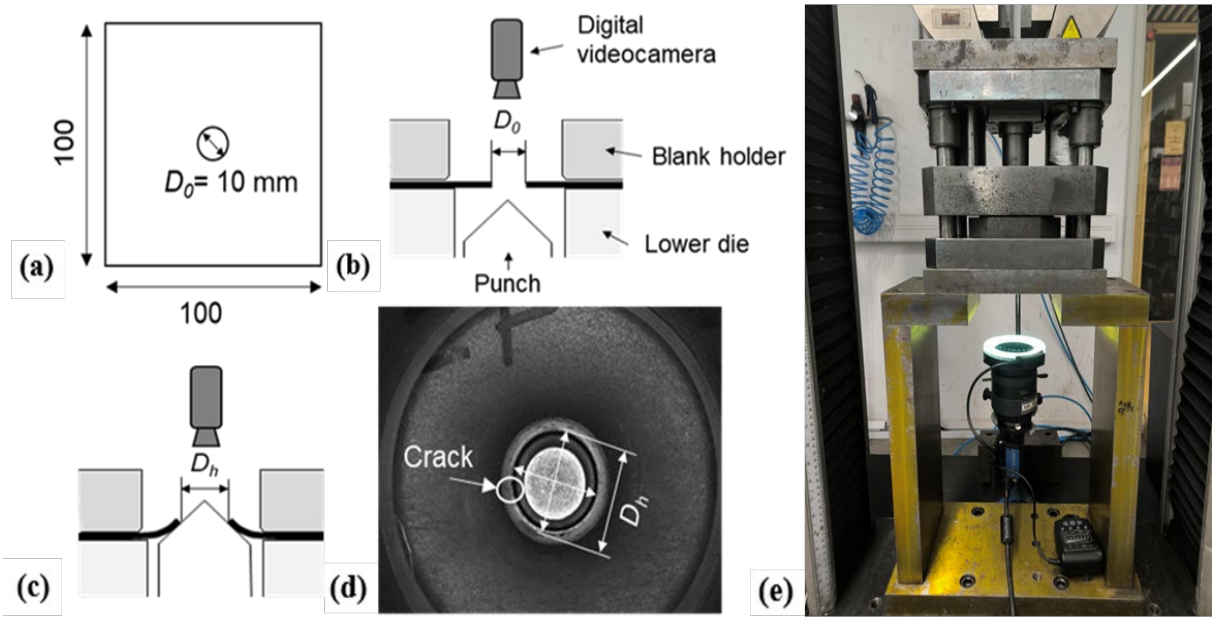

Fig. 2. (a) Specimen geometry for HET; (b- c) Schematic representation of the experimental procedure for the HET. Before (b) and after (c) the test; (d) Digital image used for the evaluation of the HER; (e) experimental setup used for the hole expansion tests.

Results and Discussion

Forming limit curves (FLCs), obtained by Nakajima testing with a 100 mm hemispherical punch and fitted using the inverse parabola procedure defined in ISO 12004-2, exhibit a differentiated response across AHSS families. The 3rd Gen grades (MMn1000 and QP980) reach higher limit strains than the 1st Gen DP1000 over the investigated range of minor strain (ε_2), with the contrast most evident around FLC_0 ($\varepsilon_2 \approx 0$) and uniaxial strain paths shown in the left hand of the Forming Limit Diagram (FLD) (Fig. 3a). This ordering is consistent with the tensile hardening capacity of the three steels: MMn1000 combines a high n-value (n = 0.25) and a wide uniform elongation (A_g = 25.7 %), QP980 follows (n = 0.19, A_g = 14.4 %), while DP1000 exhibits limited hardening (n = 0.09, A_g = 5.3 %). A higher n-value sustains strain redistribution and delays localised necking, which naturally lifts the FLC, as reported for 3rd Gen steels when compared with dual-phase grades at comparable strength levels [16] (Fig. 3b). A change in the slope of the FLC can be observed in the second quadrant in all steel grades, close to the uniaxial tension stress state. This behaviour could be attributed to a lower width-to thickness ratio of the test specimens, which tends to increase through-thickness stress effects, promoting earlier onset of localized necking. This can be especially noticeable in damage-sensitive materials, and may cause a drop in failure limits, like in the case of QP980. In the first quadrant, significant differences are observed in the slopes of the three steels. DP1000 shows a much steeper slope than QP980 and MMn1000. Such differences can be explained by the differences in work hardening of the studied steels. It has been previously reported that higher work hardening leads to lower failure limits in the first quadrant [17].

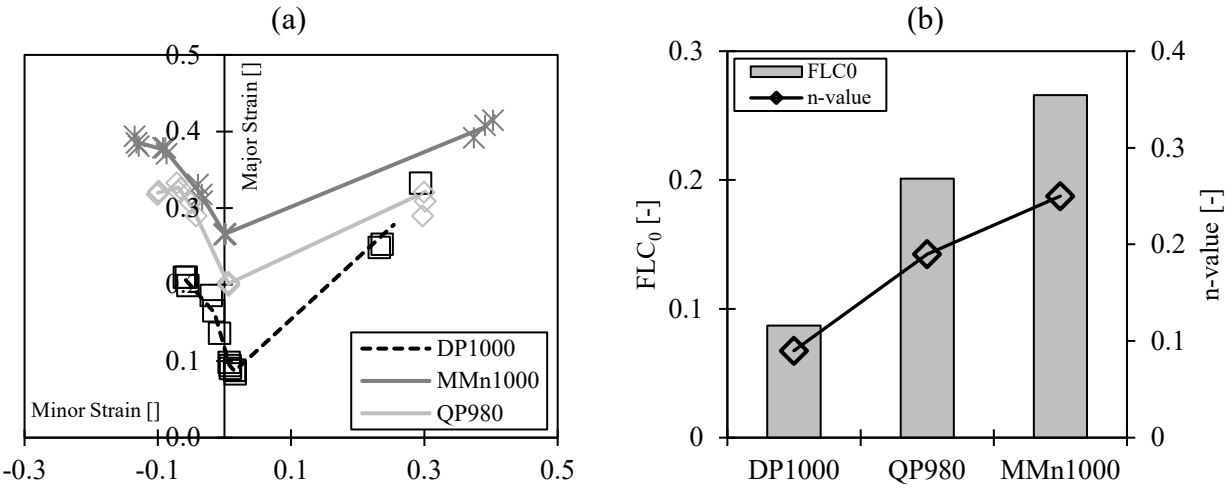

Fig. 3. (a) FLC obtained for the investigated AHSS; (b) correlation between FLC_0 values and n-values.

Local formability evaluated through the Hole Expansion Ratio (HER) underscores the critical role of edge quality. The obtained HER values for both edge preparation methods are shown in Fig.4. With punched holes, all three steels fall into similar, moderate HER values (33±2 % for DP1000, 29±0 % for QP980, 26±4 % for MMn1000). When the hole is made by EDM, HER rises sharply. DP1000 and MMn1000 reach similar (HER_{EDM} 86 %). Q&P shows a more moderate increase (HER_{EDM} = 61±6 %). These results evidence that the shear affected zone (SAZ, work-hardening, micro-voids/micro-cracks, and the burnish-fracture transition) has a major effect on edge ductility of AHSSs, reducing dramatically their hole expansion capacity. This same behaviour has been previously reported for dual-phase, complex-phase and MMn steels. It is attributed to punching-induced damage generated in the SAZ, which causes local hardening and accelerates damage accumulation and edge cracking under stretch flanging [18-20].

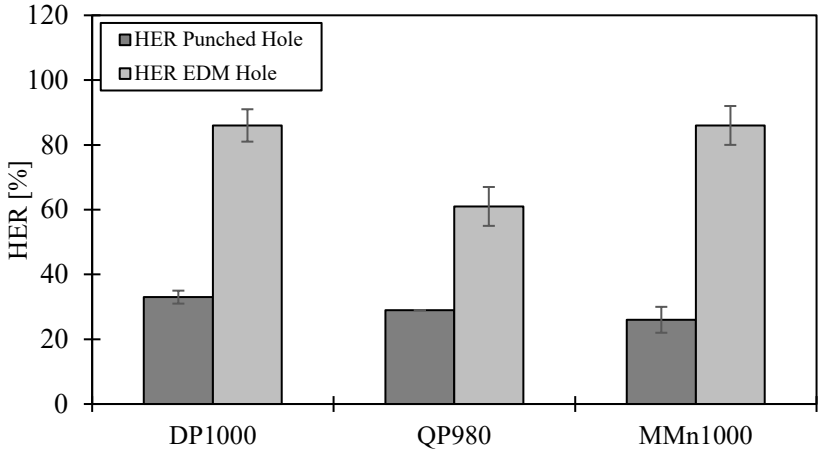

Fig. 4. Comparative analysis of Hole Expansion Ratio values for the materials studied under the two edge quality conditions.

Bringing global and local indicators together clarifies the need to evaluate both forming characteristics separately. On the one hand, global formability can be generally inferred from uniaxial tensile parameters, such as strain hardening exponent (n) or total elongation. Thus, microstructural characteristics enhancing these parameters will also have a beneficial influence on formability. As mentioned before, 3rd Gen AHSSs benefit from the strain-induced RA to martensite deformation (TRIP effect), which contributes to the formation of additional geometrically necessary dislocations, increasing strain hardening and delaying the onset of necking [21]. The beneficial influence of the TRIP effect on global ductility is directly proportional to RA volume fraction [22], which explains

the exceptional formability of the MMn steel (41% of RA) compared to Q&P (14.7% of RA) or DP1000 (2% of RA).

On the other hand, local formability modes, such as edge formability, are mainly governed by crack propagation resistance and phase hardness contrasts [18, 22], and higher RA content may have the opposite effect. During shearing/punching, the deformation induced in the SAZ, locally transforms RA to martensite, generating a hardened and more "brittle" edge [21]. When the SAZ is eliminated, as in holes machined by EDM, edge formability increases substantially. This is more evident in the case of MMn (Fig. 5a), which is the most sensitive to edge preparation method.

Fig. 5b reveals that there is no clear relationship between global and local formability indicators (FLC_0, n-value). Comparing Q&P and MMn steels, it could be said that, in the absence of a damaged SAZ, a higher resistance to localized necking (FLC_0) accompanies better edge stretchability. However, this is completely different for punched HER, where MMn exhibits the lowest value, despite having the highest FLC_0. Previous works have shown that punched HER correlates better with fracture mechanics metrics [22] and that microstructural architecture (phase fraction, distribution, and hardness mismatch) controls damage initiation and growth at the edge [18-20, 22].

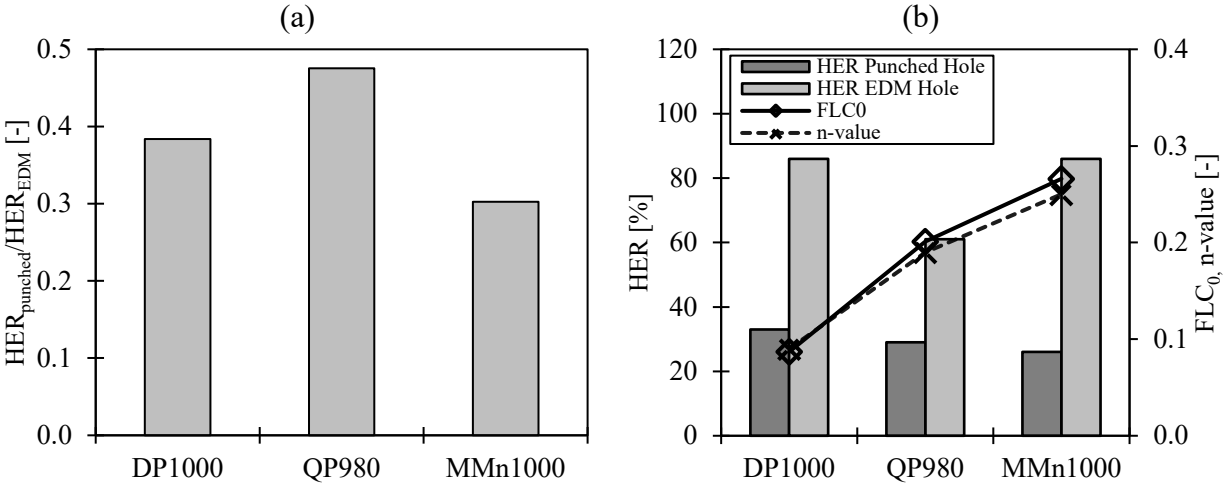

Fig. 5. (a) Ratio $HER_{punched}/HER_{EDM}$ for the investigated materials; (b) correlation between HER values and FLC_0 and n values.

From an application standpoint, these combined results suggest a simple rule of thumb. For components governed by strains homogeneously distributed in large areas, 3rd Gen grades offer a wider global window than first-generation DP steels owing to their stronger hardening and higher formability limits [16]. For stretch flanging, the outcome hinges on edge integrity. Minimizing edge damage by adopting EDM or laser, or optimizing punching (clearance, punch/die geometry, finishing) is essential to unlock local ductility potential. In the presence of cut-edge damage, fracture toughness and phase contrast management become the primary levers to raise HER [18-20, 22]. These results enhance the understanding of the differences between global and local formability in third-generation AHSSs, providing valuable insights to improve process robustness and facilitate the industrial adoption of these steels in high-performance automotive components.

Conclusion

The present investigation on the global and local formability of 3rd Gen AHSS has provided the following significant findings:

1) MMn1000 and QP980 exhibit higher forming limit strains than DP1000 across the minor strain range studied, with the largest contrast around FLC_0. This behavior is consistent with their higher strain hardening exponent and uniform elongation. In the absence of a shear affected zone (EDM holes), higher stretch flangeability is also associated with increased FLC_0.
2) Edge condition has a dominant effect on hole expansion performance. With punched edges, all grades show similar and moderate HER values. In contrast, EDM edges lead to a pronounced increase in HER, highlighting the intrinsic edge stretchability of undamaged material.

3) Damage introduced in the shear affected zone significantly reduces edge ductility, thereby limiting hole expansion capacity. Under these conditions, no direct correlation can be established between HER and global formability parameters, as failure is governed by edge damage and the material's damage tolerance. Accordingly, other parameters, such as fracture mechanics metrics, can provide better predictions.
4) From an application perspective, 3rd Gen steels provide a wider forming window for components dominated by distributed strain, whereas in stretch flanging operations, performance is primarily controlled by edge integrity. Therefore, high edge quality is essential to minimize crack initiation and premature failure.

A practical selection framework should combine both global and local formability indicators. To improve the accuracy of edge cracking predictions, edge formability should be assessed under conditions representative of the actual manufacturing process.

Acknowledgment

This work has been financially supported by the European Commission, Research Fund for Coal and Steel programme under Grant Agreement 101112540 – SUP3RFORM – RFCS-2022.

References

[1] L. Wang, J.G. Speer, Quenching and partitioning steel heat treatment, Metallo. Microstruct. Anal. 2 (2013) 268–281.

[2] W. Bleck, F. Brühl, Y. Ma, and C. Sasse, Materials and processes for the third-generation advanced high-strength steels, Berg Huettenmaenn, Monatsh 164 (2019) 466–474.

[3] H. Essoussi, S. Ettaqi, E.H. Essadiqi, From the alloy design to the microstructural and mechanical properties of medium manganese steels of the third generation of advanced high strength steels, J. Min.Metal., Sect. B-Metal. 60(3), (2024) 339–352.

[4] I. Apurwa, J.K. Yadav, A. Kumar, A perspective on third-generation medium-Mn steels for automotive application, in: S. Yadav, P.K. Jain, P.K. Kankar, Y. Shrivastava (Eds.), Advances in mechanical and energy technology, LNME, Springer, Singapore (2023) pp. 351-357.

[5] R. Pereira, N. Peixinho, S.L. Costa, A Review of Sheet Metal Forming Evaluation of Advanced High-Strength Steels (AHSS), Metals 14(4) (2024) 394.

[6] B.M. Hance, Advanced high-strength steel (AHSS) performance level definitions and targets, SAE Int. J. Mater. Manuf. 11(4) (2018) 505–516.

[7] H-h. Bok, J. Choi, Integration of local formability limits of AHSS into local/global formability map, in: K. Mocellin, P.O. Bouchard, R. Bigot, T. Balan, (Eds.) Proceedings of ICTP, LNME, Springer, Cham, 2023, pp. 435–441.

[8] B.M. Hance, Practical application of the hole expansion test, SAE Int. J. Engines 10(2) (2017) 247-257.

[9] H.-C. Shih, D. Zhou, B. Konopinski, Effects of punch configuration on the AHSS edge stretchability, SAE Int. J. Engines 10 (4) (2017) 2051-2056.

[10] F. Sun, L. Burroughs, R. Chowdhury, and M. Milliron, Effects of microstructure on hole expansion ratio of AHSS, in: International Symposium on New Developments in Advanced High-Strength Sheet Steels, AIST, Vail, CO, USA (2023).

[11] UNE-EN ISO 6892-1 Metallic materials - Tensile testing - Part 1: Method of test at room temperature (2020).

[12] ISO 12004-2 Metallic materials - Determination of forming-limit curves for sheet and strip - Part 2: Determination of forming-limit curves in the laboratory (2021).

[13] A. Payà, D. Frómeta, J. Pujante, and M. Da Silva, Effect of recycling on the mechanical properties and formability of sheet metal, Proc. IDDRG Int. Conf. 408, 02036 (2025).

[14] ISO 16630 Metallic materials - Sheet and strip - Hole expanding test (2017).

[15] D. Frómeta, M. Tedesco, J. Calvo, A. Lara, S. Molas, and D. Casellas, Assessing edge cracking resistance in AHSS automotive parts by the Essential Work of Fracture methodology. J. Phys.: Conf. Ser. 896(1), 012102 (2017).

[16] J. Noder, J.E. Gutierrez, A. Zhumagulov, J. Dykeman, H. Ezzat, and C. Butcher, A comparative evaluation of third-generation advanced high-strength steels for automotive forming and crash applications, Materials 14(17) (2021) 4970.

[17] S. Sato, M. Tsukamoto, Y. Maeda, Y. Maeda, and T. Hama, Crystal plasticity-based forming limit analysis for two types of 5052 aluminum alloy sgeets with different heat treatment conditions, Mat. Res. Proc. 41 (2024) 1009-1016.

[18] N. Habibi N, T. Beier, J. Lian, B. Tekkaya, M. Koenemann, and S. Muenstermann, Effects of damage evolution on edge crack sensitivity in dual-phase steels, Steel Res. Int. 95(10) (2024) 2400178.

[19] N. Pathak, C. Butcher, M.J. Worswick, E. Bellhouse, and J. Gao, Damage evolution in complex-phase and dual-phase steels during edge stretching, Materials 10(4) (2017) 346.

[20] P. Plosila, P. Kantanen, J. Hannula, V. Javaheri, J. Kömi, and A. Kaijalainen, Hole expansion performance of a medium manganese advanced high-strength steel after hot rolling and intercritical annealing, Mat. Res. Proc. 44 (2024) 358-367.

[21] D. Krizan, K. Steineder, S. Kaar, and T. Hebesberger, Development of third generation advanced high strength steels for automotive applications, Proc. 19th Int. Sci. Conf. Transfer (2018).

[22] D. Frómeta, A. Lara, L. Grifé, T. Dieudonné, P. Dietsch, J. Rehrl, C. Suppan, D. Casellas, and J. Calvo, Fracture resistance of advanced high-strength steel sheets for automotive applications, Metall. Mater. Trans. A 52 (2021) 840–856.